Heliyon 10 (2024) e30006

Contents lists available at ScienceDirect

Heliyon

journal homepage: www.cell.com/heliyon

Research article

# Transition of intracranial aneurysmal wall enhancement from high to low wall shear stress mediation with size increase: A hemodynamic study based on 7T magnetic resonance imaging

Yudi Tang [a,1], Haining Wei [b,1], Zihao Zhang [c,d,e,1], Mingzhu Fu [b], Junqiang Feng [a], Zhixin Li [c,d], Xinke Liu [a,f], Yue Wu [c,d], Jinyuan Zhang [c,d], Wei You [a], Rong Xue [c,d], Yan Zhuo [c,d], Yuhua Jiang [a,f], Youxiang Li [a,f,***], Rui Li [b,**], Peng Liu [a,f,*]

[a] *Department of Neurosurgery, Beijing Neurosurgical Institute and Beijing Tiantan Hospital, Capital Medical University, Beijing, China*
[b] *Center for Biomedical Imaging Research, Department of Biomedical Engineering, Medical School, Tsinghua University, Beijing, China*
[c] *State Key Laboratory of Brain and Cognitive Science, Beijing MR Center for Brain Research, Institute of Biophysics, Chinese Academy of Sciences, Beijing, China*
[d] *University of Chinese Academy of Sciences, Beijing, China*
[e] *Institute of Artificial Intelligence, Hefei Comprehensive National Science Center, Hefei, China*
[f] *Beijing Engineering Research Center, Beijing, China*

ARTICLE INFO

*Keywords:*
Aneurysm
4D flow MRI
Hemodynamics
7T MRI
Aneurysmal wall enhancement

ABSTRACT

*Background:* Wall shear stress (WSS) has been proved to be related to the formation, development and rupture of intracranial aneurysms. Aneurysm wall enhancement (AWE) on magnetic resonance imaging (MRI) can be caused by inflammation and have confirmed its relationship with low WSS. High WSS can also result in inflammation but the research of its correlation with AWE is lack because of the focus on large aneurysms limited by 3T MRI in most previous studies.This study aimed to assess the potential association between high or low WSS and AWE in different aneuryms. Especially the relationship between high WSS and AWE in small aneurysm.

*Methods:* Forty-three unruptured intracranial aneurysms in 42 patients were prospectively included for analysis. 7.0 T MRI was used for imaging. Aneurysm size was measured on three-dimensional time-of-flight (TOF) images. Aneurysm-to-pituitary stalk contrast ratio (CRstalk) was calculated on post-contrast black-blood T1-weighted fast spin echo sequence images. Hemodynamics were assessed by four-dimensional flow MRI.

*Results:* The small aneurysms group had more positive WSS–CRstalk correlation coefficient distribution (dome: 78.6 %, $p = 0.009$; body: 50.0 %, $p = 0.025$), and large group had more negative coefficient distribution (dome: 44.8 %, $p = 0.001$; body: 69.0 %, $p = 0.002$). Aneurysm size was positively correlated with the significant OSI–CRstalk correlation coefficient at the dome ($p =$

* Corresponding author. Department of Neurosurgery, Beijing Neurosurgical Institute and Beijing Tiantan Hospital, Capital Medical University, Beijing, China.
** Corresponding author. Center for Biomedical Imaging Research, Department of Biomedical Engineering, Medical School, Tsinghua University, Beijing, China.
*** Corresponding author. Department of Neurosurgery, Beijing Neurosurgical Institute and Beijing Tiantan Hospital, Capital Medical University, Beijing, China.
*E-mail addresses:* liyouxiang@mail.ccmu.edu.cn (Y. Li), leerui@tsinghua.edu.cn (R. Li), skeletonliu@sina.com (P. Liu).
[1] Yudi Tang, Haining Wei and Zihao Zhang have contributed equally to this work.

https://doi.org/10.1016/j.heliyon.2024.e30006
Received 15 November 2023; Received in revised form 11 April 2024; Accepted 18 April 2024
Available online 23 April 2024

0.012) and body ($p = 0.010$) but negatively correlated with the significant WSS–CRstalk correlation coefficient at the dome ($p < 0.001$) and body ($p = 0.017$).
*Conclusion:* AWE can be mediated by both high and low WSS, and translate from high WSS- to low WSS-mediated pathways as size increase. Additionally, AWE may serve as an indicator of the stage of aneurysm development via different correlations with hemodynamic factors.

## 1. Introduction

Intracranial aneurysms are common [1,2]. Although many never rupture, ruptured aneurysms are the most common cause of subarachnoid hemorrhage [2–4], which is associated with high mortality and morbidity [3–5]. Inflammation in the aneurysmal wall has been found to be associated with aneurysm development and rupture [6,7]. Aneurysm wall enhancement (AWE) visualized on magnetic resonance imaging (MRI) of unruptured intracranial aneurysms (UIAs) is considered a biomarker of inflammation [8–10] and an indicator of higher risk of growth and rupture [11,12].

It has been reported that AWE was negatively correlated with the spatial distribution of wall shear stress (WSS) and positively correlated with oscillatory shear index (OSI) [8]. Compared to non-enhanced areas, areas of AWE have lower WSS and higher OSI [8, 13]. And this phenomenon is usually explained by local inflammation caused by low WSS [14]. However, aneurysmal wall inflammation is also found to be associated with high WSS which induces destruction and weakening of vessel walls [15]. It seemed that AWE could be also caused by high WSS.

Can et al. [16] conducted a systematic review and meta-analysis on the association between hemodynamic factors and the formation and rupture of intracranial aneurysms. Their findings suggest that low WSS is significantly associated with an increased risk of aneurysm rupture. Furthermore, they observed that higher WSS and an elevated gradient oscillatory number may contribute to the formation of aneurysms. However, most aneurysms in previous studies [8,12,13,17,18] were large (size>4 mm). Small (size<4 mm) aneurysms, which seems to be associated with the formation stage, were lack of exploration individual. Therefore, positively correlated between AWE and WSS in most small aneurysms might be ignored.

Meng et al. [19]. reviewed previous studies, including hemodynamic and pathological specimens, and proposed that aneurysms could transition from high WSS mediated inflammation pathway to low WSS mediated inflammation pathway in anueyrsms formation, growth and rupture. And this phenomenon is predicted to be observed in changes in aneurysm size. Therefore, we assumed that AWE could be observed a transition from high-mediated to low WSS- mediated with aneurysm size increase.

In this study, the 7T MRI was used to study the quantitative relationship between AWE distribution and hemodynamic parameters in UIAs, since the 7T MRI could provide better images with a higher signal-to-noise ratio and higher resolution than 3T MRI [4,20,21], which allows a better characterization of AWE and hemodynamics, especially in small aneurysms. In detail, the aneurysm-to-pituitary stalk contrast ratio (CRstalk) was utilized to quantify the AWE [22]. And a quantification workflow proposed by Fu et al. [8]. was used to explore the relationships among AWE, hemodynamics, and aneurysm size.

## 2. Methods

This study was approved by the local institutional ethics committee.

## 3. Study population

All participants provided written informed consent. Patients with UIAs were recruited from September 2020 through March 2023. UIAs were diagnosed by magnetic resonance angiography (MRA), computed tomography angiography, or digital subtraction angiography. Inclusion criteria were as follows: 1) no contraindication to 7 T MRI, 2) ability to cooperate during the MR examination and 3) no contraindication to gadolinium-based contrast agent. Patients with fusiform, dissecting, thrombosed aneurysms, or irregular aneurysms were excluded. Patients were also excluded with images of poor quality. Aneurysms located at the anterior cerebral artery (ACA) or anterior communicating artery (AComA) were excluded from this study since their special hemodynamic environment [23] and anatomical structure [24,25].

## 4. Imaging protocol

MRI imaging was performed using a 7.0 T system (Magnetom Terra, Siemens, Munich, Germany) equipped with a Nova 32-channel head coil. Sequences included three-dimensional (3D) time-of-flight MRA (TOF-MRA), pre- and post-contrast black-blood SPACE (fast spin echo with variable flip angle trains [20]), and four-dimensional flow MRI (4D-flow MRI) [26]. 3D TOF-MRA was used to locate the aneurysm and assess its geometry. Imaging parameters were as follows: repetition time/echo time (TR/TE), 18/4.08 ms; field of view (FOV), 211 × 168 $mm^2$; voxel size, 0.33 × 0.33 × 0.40 $mm^3$; and flip angle, 23°. Pre- and post-contrast high-resolution MRI imaging parameters were as follows: TR/TE, 1200/13 ms; FOV, 179 × 179 $mm^2$; voxel size, 0.40 × 0.40 × 0.40 $mm^3$; and echo train length (ETL), 40. Post-contrast high-resolution MRI was performed 15 min after injection of a gadolinium-based contrast agent (Omniscan TM; GE Healthcare, Chicago, IL, USA) into an antecubital vein (0.1 mmol/kg dose at 5 mL/s). 4D-flow MRI was acquired using a free-breathing, peripheral pulse-gated multi-shot turbo field echo sequence with the following parameters: TR/TE, 60.88/3.68 ms;

FOV, 192 × 192 $mm^2$; voxel size, 0.60 × 0.60 × 0.80 $mm^3$; flip angle, 15°; and velocity encoding (VENC), 150 cm/s. Reformatting all sequences to any plane was possible during image processing.

## 5. Assessment of CRstalk and hemodynamics

To examine the relationship between CRstalk and hemodynamic parameters, a workflow reported by Fu. et al. [8] was utilized to obtain the quantification results, as shown in Fig. 1 (A - F). Firstly, benefit from the high velocity-noise-ratio of 4D-flow MRI magnitude images, the 3D vessel model was generated using the time-averaged 4D-flow magnitude images, rather than 3D TOF-MRA in previous studies. Various algorithms such as threshold segmentation, region growth, connected domain selection and surface

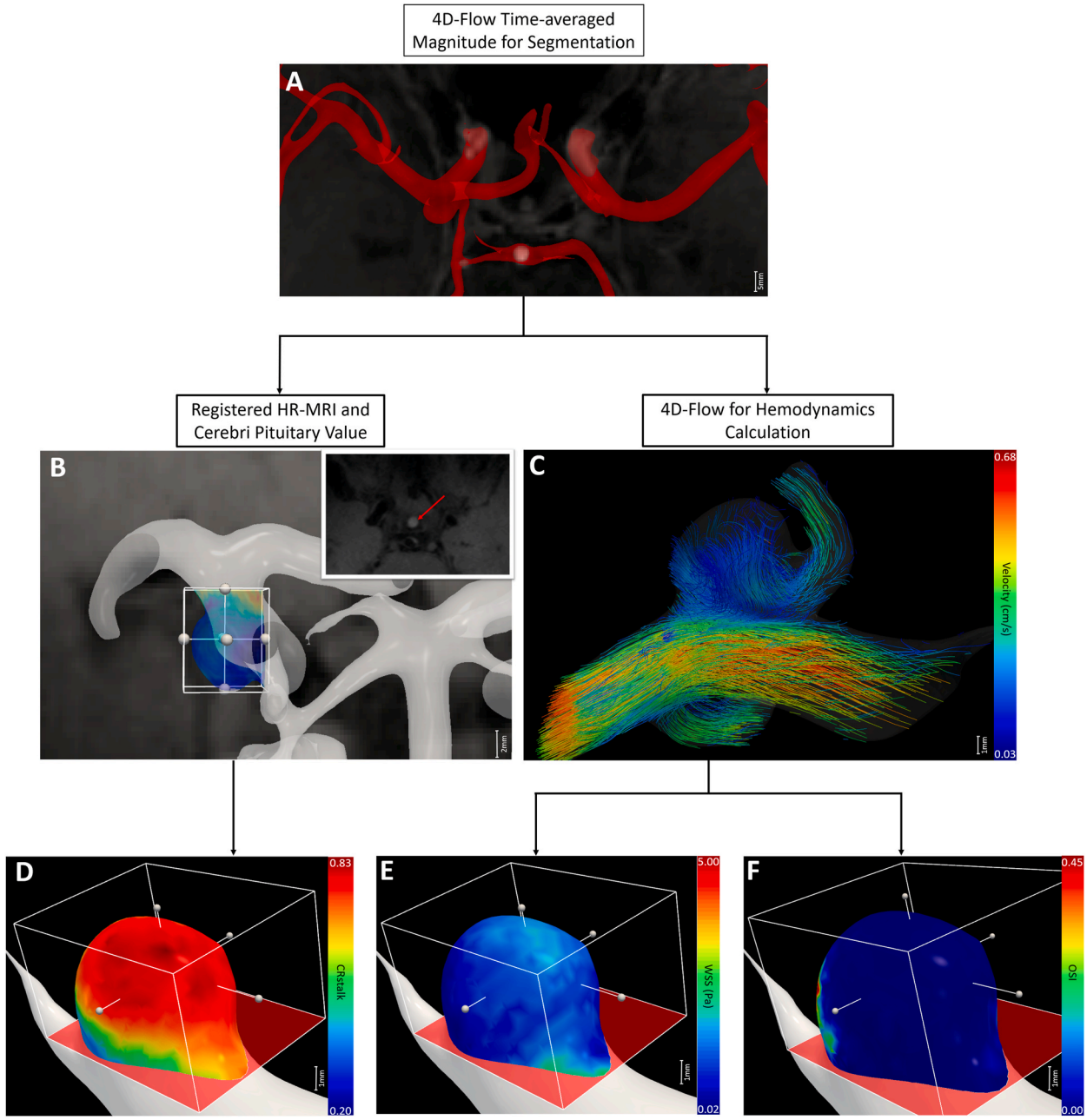


**Fig. 1.** Workflow for assessment of CRstalk and hemodynamic parameters. (A) 3D model of aneurysm was generated by threshold segmentation of time-averaged 4D flow magnitude. Manually select the appropriate threshold and keep the maximum component. (B) Registered post-contrast HR-MRI was used to obtain the pituitary intensity. (C) 3D velocity streamline calculated from 4D flow MRI. (D–F) Spatial distribution of CRstalk, WSS and OSI.

smoothing were applied to accomplish this step. Subsequently, in order to calculate CRstalk [22], we employed an automatic volumetric rigid registration method within 3D Slicer software (www.slicer.org) to align post-contrast HR-MRI scans with the 4D-flow MRI data. The image signal intensity from post-contrast HR-MRI was projected onto the 3D vessel model asaneurysm wall intensity. This projection was performed by the maximum signal intensity along a line perpendicular to each mesh node on vessel model. Meanwhile, the intensity of the pituitary stalk was also calculated through post-contrast HR-MRI. CRstalk was calculatedas the quotient of aneurysm wall signal intensity/pituitary stalk signal intensity. Finally, hemodynamic analysis was performed through 4D-flow phase imaging and corresponding velocity mask. The streamline was plotted to ensure the blood flow inner aneurysm had accurate velocity results. Then, the time-averaged WSS and OSI were calculated using the obtained WSS during a cardiac cycle. The measurement of CRstalk was shown in Fig. 2 (A - F).

WSS was calculated by following equation, where μ means the dynamic viscosity and y means the distance to the wall.

$$WSS - \boldsymbol{\mu}\left(\frac{\partial v_{parallel}}{\partial y}\right) y = 0$$

OSI, denoting the fluctuation of WSS was calculated with formula.

$$OSI = 0.5\left(1 - \frac{\left|\int_0^T WSSdt\right|}{\int_0^T |WSS|dt}\right)$$

## 6. Aneurysm classification

According to the correlation between WSS and CRstalk, aneurysms were divided into positive group, negative group, and non-significant ($p < 0.05$) group. Aneurysm morphology was measured on 7 T images using 3D Slicer 4.10.1 (http://www.slicer.org). The size of UIAs was defined as their largest diameter measured on the maximum intensity projection of TOF images. And the aneurysms were classified into small (≤4 mm) group and large (>4 mm) group. By the distance to the aneurysm neck, each aneurysm was subdivided into three subregions [27]: neck, body, and dome, as shown in Fig. 3 (A - B). The neck of aneurysms would not participate in the comparison because of the interference of the parent artery [28].

## 7. Statistical analysis

Statistical analyses were conducted using SPSS software version 26.0 (IBM Corp., Armonk, NY, USA). The normality of data distribution was tested using the Kolmogorov–Smirnov and Shapiro–Wilk methods. Correlation was examined using Pearson's or

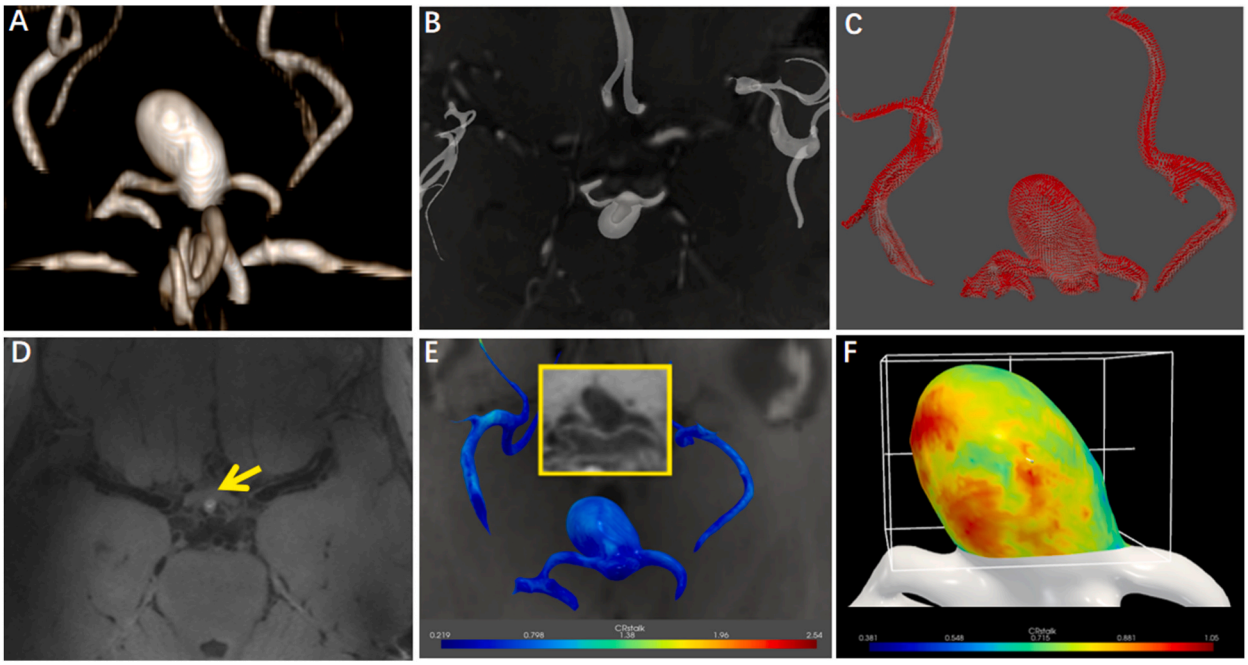


**Fig. 2.** Illustration of CRstalk measurement. A: The maximum intensity projection from DICOM images. B:The 3D vessel model from time averaged 4D-flow images. C: the norm vectors perpendicular to each mesh node on vessel model. D: Obtain the signal intensity of the pituitary stalk. The yellow arrow points to the pituitary stalk. E: Mapping the quotient of maximum signal intensity along norm vectors and pituitary stalk signal intensity to the vessel model. The yellow frame shows the post-contrast HR-MRI image. F: Corresponding distribution map of CRstalk.

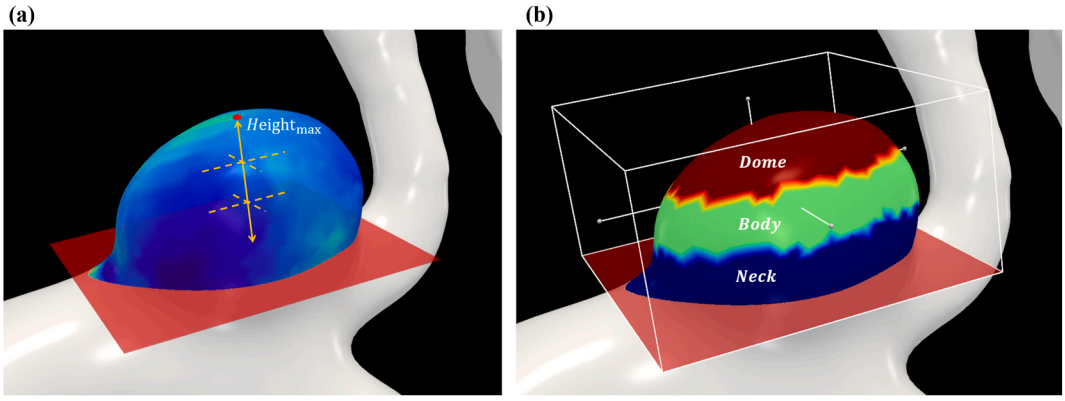


**Fig. 3.** Subregions of each aneurysm. (a) Red plane represents the neck of aneurysm. The yellow arrow represent the maximum distance from the neck plane, and is divided into three equal parts. (b) According to the height of each section, the aneurysm is divided into three areas: neck, body, and dome.

Spearman's method according to distribution type. Chi-Square Pearson test, correction for continuity and Fisher's exact test were used to compare AWE and hemodynamic parameters between small and large aneurysms. $P < 0.05$ was considered significant.

## 8. Results

Finally forty-three UIAs in 42 patients were included in this study. 26 aneurysms were located at anterior circulation and 17 aneurysms were located at posterior circulation. Patient characteristics are shown in Table 1. Data of mean CRstalk, mean WSS, mean OSI and aneurysm size were not distributed normally among all aneurysms. A flow chart was shown in Fig. 4.

## 9. Inter- and intra-group relationship

Correlation between hemodynamic parameters and CRstalk was significant in most aneurysms. WSS was significantly correlated with CRstalk at dome in 33 aneurysms (76.7 %) and at body in 34 aneurysms (79.1 %). At dome region, 20 aneurysms were classified into the positive group and 13 aneurysms were classified into the negative group. And at body region, 12 aneurysms were included in positive group and 22 aneurysms were included in negative group. The relationship between OSI and CRstalk was significant at dome in 31 aneurysms 72.1 % and at body in 34 aneurysms (79.1 %). Furthermore, it was shown that these relationships may differ at dome and body region even though on the same aneurysm. More details were shown in Supplemental Table 1.

Among all aneurysms, mean OSI was positively associated with aneurysm size in dome and body regions, as shown in Table 2. It was also shown that there was a negative relationship between mean WSS and mean OSI in both two regions. However, neither mean WSS nor OSI was significantly correlated with CRstalk.

**Table 1**
Patient characteristics of the study population (n = 42).

| Parameter | |
|---|---|
| Age ≥ 60 years, n (%) | 23 (54.8 %) |
| Gender-male, n (%) | 22 (52.4 %) |
| Gender-female, n (%) | 20 (47.7 %) |
| Hypertension, n (%) | 34 (81.0 %) |
| Diabetes, n (%) | 6 (14.3 %) |
| Smoking, n (%) | 16 (38.1 %) |
| Drinking, n (%) | 12 (28.6 %) |
| Mean LDL (±SD)*,mmol/L | 2.30 (±0.73) |
| Mean HDL (±SD)*,mmol/L | 1.36 (±0.17) |
| Mean TG (±SD)*,mmol/L | 1.35 (±0.76) |
| Mean TC (±SD)*,mmol/L | 4.28 (±0.74) |
| Mean aneurysm size (±SD), mm | 6.07 (±2.99) |
| Mean aneurysm neck width (±SD), mm | 4.89 (±1.73) |

Abbreviations: SD:standard deviation; LDL:low-density lipoprotein; HDL: high-density lipoprotein; TG:triglyceride; TC:total cholesterol.
*: Data provided by patients based on their last examination results before MRI scan.

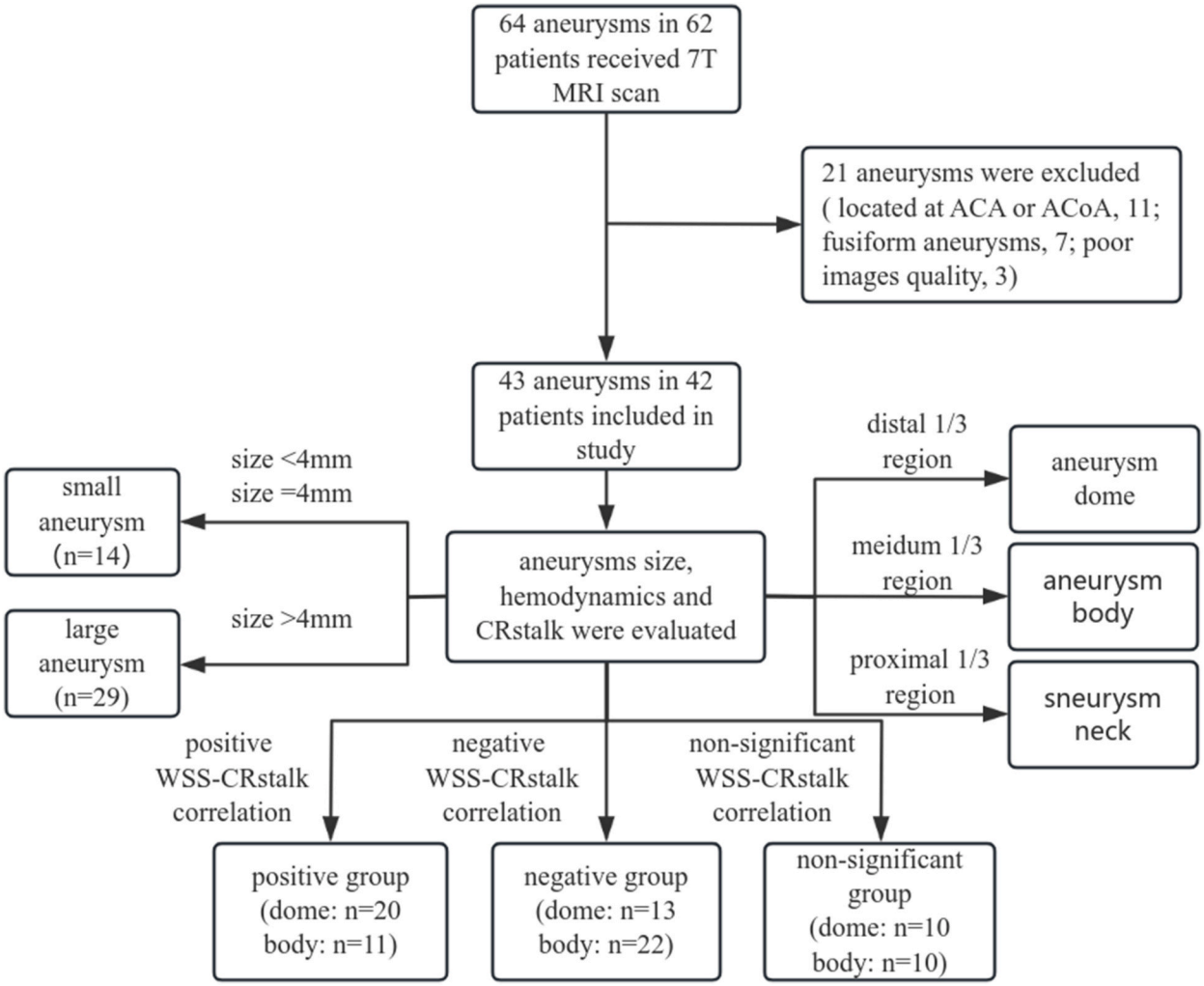


**Fig. 4.** Flowchart of this study.

**Table 2**
Correlations between size, mean hemodynamics and CRstalk in the dome and body.

| Correlation | Dome | p | Body | p |
|---|---|---|---|---|
| Size and individual WSS-CRstalk* | −0.591 | <0.001 | −0.406 | 0.017 |
| Size and individual OSI-CRstalk* | 0.447 | 0.012 | 0.435 | 0.010 |
| mean WSS and mean CRstalk | 0.055 | 0.727 | −0.027 | 0.866 |
| mean OSI and mean CRstalk | −0.120 | 0.444 | −0.080 | 0.611 |
| mean WSS and mean OSI | −0.823 | <0.001 | −0.826 | <0.001 |
| Size and mean CRstalk | 0.165 | 0.291 | 0.230 | 0.138 |
| Size and mean WSS | −0.206 | 0.184 | −0.76 | 0.073 |
| Size and mean OSI | 0.367 | 0.016 | 0.350 | 0.021 |
| Size and individual WSS-CRstalk | −0.499 | 0.001 | −0.506 | 0.001 |
| Size and individual OSI-CRstalk | 0.443 | 0.003 | 0.410 | 0.006 |

*non-significant($p \geq 0.05$) individual hemodynamics-CRstalk were excluded.

## 10. Aneurysm size in positive, negative group and non-significant group

As in Fig. 5 (A - B), the medium aneurysm size at aneurysm dome was 3.89 mm (25 %,75 %:3.50,6.60) in positive group, 6.33 mm (25 %,75 %:5.39,9.82) in negative group, and 4.76 mm (25 %,75 %:3.71,8.48) in non-significant group, respectively. And at aneurysm body, medium aneurysm size was 3.85 mm (25 %,75 %:3.49,4.91) in positive group,7.34 mm (25 %,75 %:6.05,8.97) in negative group, and 3.91 mm (25 %,75 %:3.72,4.96) in non-significant group.

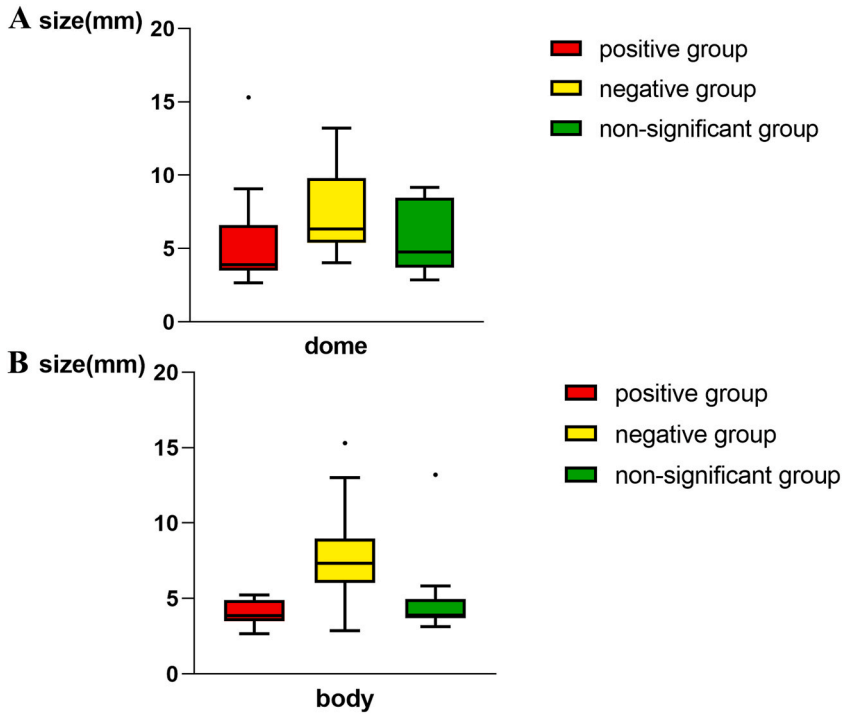


**Fig. 5.** Distribution of the aneurysm maximum diameter in negative group, non-significant group and positive group at dome and body. A: Distribution at aneurysm dome. B: Distribution at aneurysm dome.

Aneurysm size in positive group was significantly smaller than that of negative group at both dome region ($p = 0.008$) and body region ($p < 0.001$). Although the aneurysm size in non-significant group was smaller than in negative group at body ($p = 0.009$), there was no significant difference with in negative group at dome ($p = 0.172$), and positive group at dome ($p = 0.344$) and body ($p = 0.522$) region.

## 11. Relationship in aneurysms with different size

Based on the above-mentioned results, it was hinted that there may be a significant association between the WSS– and OSI–CRstalk correlation coefficients and aneurysm size. As shown in Table 3, the small group had more positive WSS–CRstalk correlation coefficient distribution (dome: 78.6 %, $p = 0.009$; body: 50.0 %, $p = 0.002$) and large group had more negative coefficient distribution (dome: 51.7 %, $p = 0.001$; body: 69.0 %, $p = 0.002$). In contrast, the OSI–CRstalk correlation coefficient was usually negative in small aneurysms (dome: 64.3 %, $p = 0.002$; body: 50.0 %, $p = 0.025$) and positive in large ones (dome: 51.7 %, $p = 0.025$, body: 69.0 %, $p = 0.009$).

**Table 3**
Comparison of dome and body between the small (≤4 mm) group and large (>4 mm) group.

| subregion | Hemodynamics-CRstalk | correlation | size≤4 mm (n = 14) | size>4 mm (n = 29) | p | p* |
|---|---|---|---|---|---|---|
| dome | WSS-CRstalk | Negative | 0.0 % | 44.8 % | 0.002 | 0.001 |
| | | Positive | 78.6 % | 31.0 % | | 0.009 |
| | | Non-significant | 21.4 % | 24.1 % | | 1.000 |
| | OSI-CRstalk | Negative | 64.3 % | 20.7 % | 0.005 | 0.005 |
| | | Positive | 7.1 % | 51.7 % | | 0.013 |
| | | Non-significant | 28.6 % | 27.6 % | | 1.000 |
| body | WSS-CRstalk | Negative | 14.3 % | 69.0 % | 0.002 | 0.002 |
| | | Positive | 50.0 % | 17.2 % | | 0.025 |
| | | Non-significant | 35.7 % | 13.8 % | | 0.122 |
| | OSI-CRstalk | Negative | 50.0 % | 17.2 % | 0.018 | 0.025 |
| | | Positive | 21.4 % | 65.5 % | | 0.017 |
| | | Non-significant | 28.6 % | 17.2 % | | 0.649 |

p: Compare the distribution of three correlations between the two groups.
P*:Compare the distribution of correlation between the two groups.

## 12. Correlation between size and hemodynamics-CRstalk correlation-coefficient

As shown in Fig. 6 (A - D), the aneurysm size was positively correlated with the significant OSI–CRstalk correlation-coefficient at the dome ($r = 0.447$, $p = 0.012$) and body ($r = 0.435$, $p = 0.010$) but negatively correlated with the significant WSS–CRstalk correlation-coefficient at the dome ($r = -0.591$, $p < 0.001$) and body ($r = -0.406$, $p = 0.017$).

## 13. Discussion

The association between CRstalk and hemodynamics in UIAs was variable and seemed to have no constant value of correlation coefficient. Compared with previous studies [8,13,28], our findings in large aneurysms were similar; however, they were different in small aneurysms. In our study, AWE was stronger in regions with lower WSS and higher OSI in large aneurysms but was stronger in regions of higher WSS and lower OSI in small aneurysms. However, these findings were not contradictory, but rather consistent with the two different WSS-inflammation pathway. Furthermore, the results that the hemodynamics were associated with the aneurysm size met the previous studies [29–31] and the assumption in our study.

The region with higher WSS in small aneurysms had higher CRstalk, indicating that AWE in these aneurysms can be mediated by high WSS. This result was not surprising and can be explained by the high WSS theory. High WSS could cause endothelial injury, wall remodeling and degeneration, and overproduction of nitric oxide (NO), which results in decreased arterial tone and apoptosis of smooth muscle cells in vessel walls [32,33]. The combination of increased NO, wall stretching, and high WSS could result in inflammation [15,32], which appears as AWE on imaging. Meng et al. [19] reported that small aneurysms usually had uniformly thin, smooth, hypocellular, and translucent walls and hypothesized a high WSS-driven mural cell-mediated pathway. Induction of high WSS

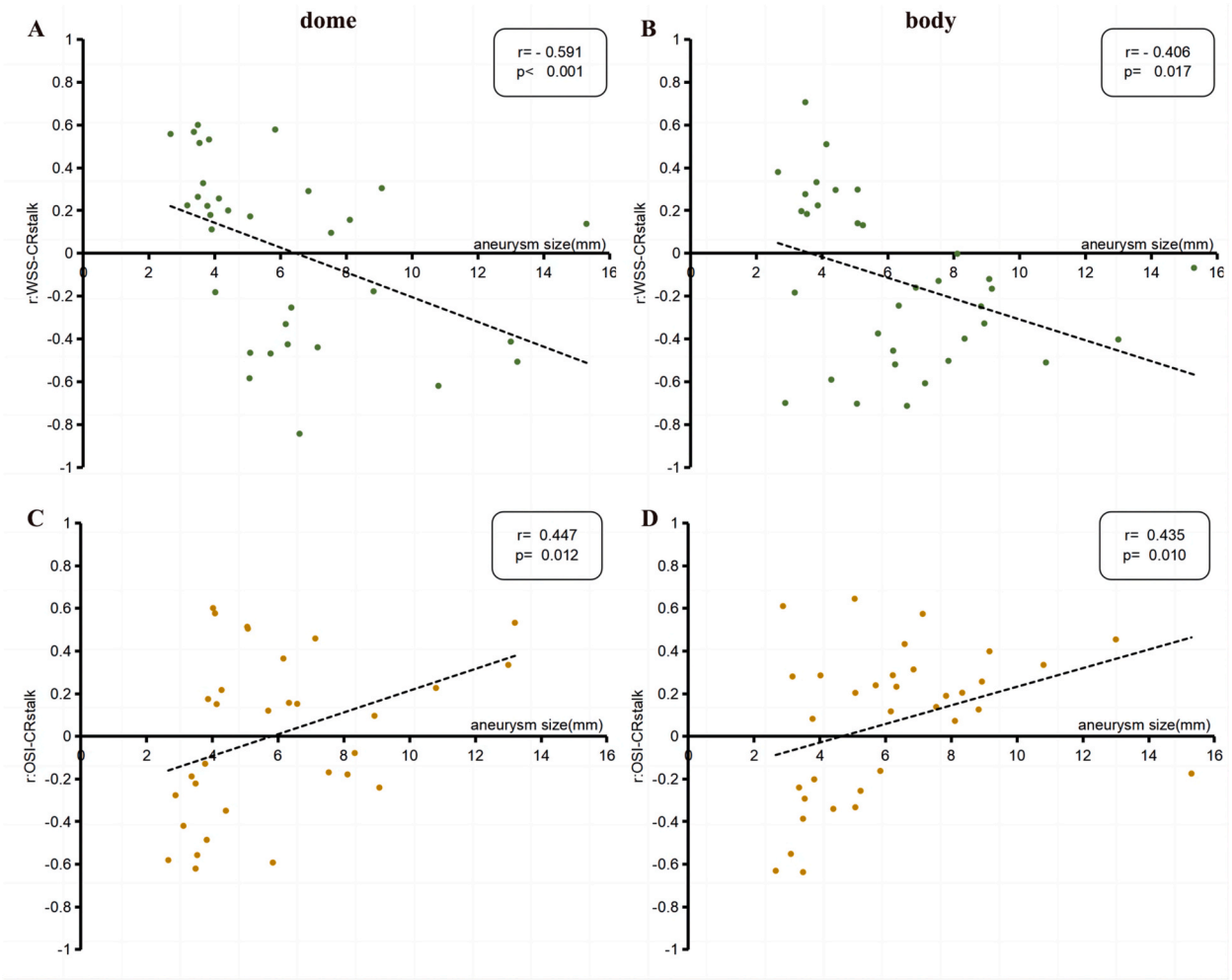


**Fig. 6.** Correlation between size and the r value of hemodynamics-CRstalk. A: Correlation between size and the r value of WSS-CRstalk at aneurysm dome. B: Correlation between size and the r value of WSS-CRstalk at aneurysm body. C: Correlation between size and the r value of OSI-CRstalk at aneurysm dome. D: Correlation between size and the r value of OSI-CRstalk at aneurysm body.

could initiate UIA formation [34,35] and maintain their development [15,36]. We hypothesized that the aneurysmal wall inflammation caused by high WSS may be a mediating mechanism, as the positive correlation found between CRstalk and WSS in the samll aneurysms.

The negative correlation between WSS and AWE in large aneurysms can be explained by low WSS theory. Low WSS and high OSI is known to elicit an inflammatory response in the endothelium [19,32] and thicken the aneurysm wall [19,37–39]. In our study, it was found that CRstalk was higher in regions with lower WSS in large aneurysms. Therefore, it was believed that these findings were consistent with the phase of UIA development. In addition, the non-significant relationship may reflect the conversion or mixing of positive correlation and negative correlation in such aneurysm regions, especially the non-significant group seems larger than positive group and smaller than negative group and the opposite WSS-CRstalk relationship can be found in the same aneurysm. However, this hypothesis needs further exploration.

Previous studies usually focused on large aneurysms and believed that lower WSS was associated with AWE. Fu et al. [8] found that the spatial distribution of WSS was negatively correlated with AWE and OSI was positively correlated with AWE in most aneurysms with AWE. However, aneurysms smaller than 4 mm were excluded in this study. Zhang et al. [9]. had the similar result that a low WSS and low average vorticity were independently associated with a high AWE grade for IAs larger than 4 mm. Obviously, their researchs lack the relationship between hemodynamics and AWE in small aneurysms. In addition, many previous studies [13,17,18] have mixed large and small aneurysms to study the relationship between hemodynamics and AWE, which will mask the different hemodynamics–AWE correlation in small aneurysms especially with much more large aneurysm than small aneurysm.

Although both high WSS and low WSS can cause inflammation and lead to instability of the aneurysm wall, WSS cannot be considered irrelevant. High and low WSS can cause inflammation through different mechanisms, resulting in different phenotypes. Meng et al. [19]. reviewed previous research data and found that there are two basic type aneurysm. At one extreme is the small thin-walled phenotype; at the other extreme is the large thick-walled phenotype; and in between is a continuum representing an amalgamation of these 2 basic types. Small thin-walled phenotype is associated with high WSS and large thick-walled phenotype usually associated with low WSS. According to intraoperative observations [19,40], UIAs gradually change from small (<4 mm) thin-walled aneurysms to large (>10 mm) thick-walled ones. In addition, this continuous change in appearance with size is consistent with the CRstalk–WSS correlation with size in our study. Therefore, we have enough reason to believe that the gradual transformation of WSS-CRstalk correlation from positive correlation to negative with increasing size is not a numerical coincidence.

The mechanism that AWE mediated by high WSS transfer to low WSS during UIAs size increase may be related to hemodynamic changes caused by size increase. Meng et al. [34]. submited a concept that aberrant hemodynamics including both high WSS and low WSS can tip the balance between maintains vascular homeostasis and drive destructive remodeling and show us corresponding manifestation aneurysm until ruptured or a new balance is created. At the iniation of aneurysms, high WSS plays a important role in formation and matain, and show us positive WSS-CRstalk correlation. As the size of intracranial aneurysms increases, WSS usually decreases [41] and may tip the balance, resulting in AWE correlated with low WSS in most aneurysms. However, the variability of hemodynamic changes between aneurysms is large and not absolutely consistent [30]. This may also explain why AWE is positively correlated with WSS in some large aneurysms and negatively correlated with WSS in some small aneurysms. In addition, there is no widely accepted threshold for determining whether WSS is high and low. Therefore, measuring the correlation between WSS and CRstalk is a reliable method to evaluate the development trend and risk of aneurysms. Furtermore, different relationships can exist at different regions of the same aneurysm. Accurate assessment of regional WSS-CRstalk correlation may help us predict the rupture point or growth area of aneurysms.

ACA and AcomA aneurysms are different from those in other locations, as they are characterized by small size and lower WSS at the time of rupture [42–44]. Castro et al. [45] studied the relationship between hemodynamics and rupture of AcoA aneurysms >4 mm in size and found that WSS was higher in ruptured aneurysms than unruptured ones. The unique hemodynamic environment and anatomical structure of ACA and AcoA aneurysms may explain their differences from other aneurysms [19,23–25]. Compared with the hemodynamics of the aneurysmal dome and body, hemodynamics at the neck are more similar to those of the parent artery [28,46]. For similar reasons, the correlations were stronger between WSS– and OSI–CRstalk correlations and size at the dome than at the body.

## 14. Limitations

This study has several limitations. Firstly, the inclusion criteria were strict and therefore the findings may do not apply to all aneurysms. Secondly, aneurysmal wall enhancement in MRI images can not only be caused by aneurymal inflammation. In serval studies, aneurysmal pseudo-enhancement signals could be caused by the near-wall slow flow and interfered with the results. Although the method of sampling signal intensities outward aneurysmal wall [17] was taken to reduce the such impact of pseudo-enhancement, a more refined approach was needed to eliminate this confusion in further study. Lastly, the pathological examination of aneurysms was not performed to confirm the conjecture.

## 15. Conclusion

AWE can be mediated by both high and low WSS, and translate from high WSS- to low WSS-mediated pathways as size increase. Additionally, AWE may serve as an indicator of the stage of aneurysm development via different correlations with hemodynamic factors.

## Funding

National Natural Science Foundation of China (81901197), National Natural Science Foundation of China (82171289),National Natural Science Foundation of China (82001804), Youth Innovation Promotion Association CAS (2022093), Natural Science Foundation of Beijing Municipality (7191003), Ministry of Science and Technology of China grant (2019YFA0707103), R&D Program of Beijing Municipal Education Commission (KM202210025013)

## Ethical approval

Beijing Tiantan Hospital, Capital Medical University.

## Informed consent

All participants provided written informed consent.

## Guarantor

Peng Liu.

## Data availability

Data will be made available on reasonable request.

## CRediT authorship contribution statement

**Yudi Tang:** Writing – original draft, Visualization, Formal analysis, Conceptualization. **Haining Wei:** Visualization, Software, Formal analysis. **Zihao Zhang:** Investigation, Funding acquisition, Data curation. **Mingzhu Fu:** Validation, Software. **Junqiang Feng:** Resources, Investigation. **Zhixin Li:** Investigation, Data curation. **Xinke Liu:** Investigation. **Yue Wu:** Investigation, Data curation. **Jinyuan Zhang:** Investigation, Data curation. **Wei You:** Investigation. **Rong Xue:** Investigation, Data curation. **Yan Zhuo:** Investigation, Data curation. **Yuhua Jiang:** Investigation. **Youxiang Li:** Project administration. **Rui Li:** Software, Methodology. **Peng Liu:** Writing – review & editing, Supervision, Methodology, Funding acquisition.

## Declaration of competing interest

The authors declare the following financial interests/personal relationships which may be considered as potential competing interests: Peng Liu reports financial support was provided by National Natural Science Foundation of China. Zihao Zhang reports financial support was provided by National Natural Science Foundation of China. Youxiang Li reports financial support was provided by National Natural Science Foundation of China. Zihao Zhang reports financial support was provided by Youth Innovation Promotion Association CAS. Zihao Zhang reports financial support was provided by Natural Science Foundation of Beijing Municipality. Zihao Zhang reports financial support was provided by Ministry of Science and Technology of China grant. Xinke Liu reports financial support was provided by R&D Program of Beijing Municipal Education Commission. If there are other authors, they declare that they have no known competing financial interests or personal relationships that could have appeared to influence the work reported in this paper.

## Acknowledgments

The authors acknowledge Dongbiao Sun and Dixuan Wu (Institute of Biophysics, Chinese Academy of Sciences) for their contribution to MRI data acquisition. Partial technical support for the imaging optimization was provided by Dr. Jing An (Siemens Shenzhen Magnetic Resonance Ltd).

## Appendix A. Supplementary data

Supplementary data to this article can be found online at https://doi.org/10.1016/j.heliyon.2024.e30006.

## References

[1] M. Vlak, A. Algra, R. Brandenburg, G. Rinkel, Prevalence of unruptured intracranial aneurysms, with emphasis on sex, age, comorbidity, country, and time period: a systematic review and meta-analysis, Lancet Neurol. 10 (2011) 626–636, https://doi.org/10.1016/s1474-4422(11)70109-0.

[2] J. van Gijn, R. Kerr, G. Rinkel, Subarachnoid haemorrhage, Lancet (London, England) 369 (2007) 306–318, https://doi.org/10.1016/s0140-6736(07)60153-6.

[3] S. Juvela, K. Poussa, H. Lehto, M. Porras, Natural history of unruptured intracranial aneurysms: a long-term follow-up study, Stroke 44 (2013) 2414–2421, https://doi.org/10.1161/strokeaha.113.001838.

[4] S. Neifert, E. Chapman, M. Martini, W. Shuman, A. Schupper, E. Oermann, J. Mocco, R. Macdonald, Aneurysmal subarachnoid hemorrhage: the last decade, Translational stroke research 12 (2021) 428–446, https://doi.org/10.1007/s12975-020-00867-0.

[5] E. Leemans, B. Cornelissen, M. Sing, M. Sprengers, R. van den Berg, Y. Roos, W. Vandertop, C. Slump, H. Marquering, C. Majoie, 7T versus 3T MR angiography to assess unruptured intracranial aneurysms, J. Neuroimaging : official journal of the American Society of Neuroimaging 30 (2020) 779–785, https://doi.org/10.1111/jon.12772.

[6] P. Liu, H. Qi, A. Liu, X. Lv, Y. Jiang, X. Zhao, R. Li, B. Lu, M. Lv, H. Chen, Y. Li, Relationship between aneurysm wall enhancement and conventional risk factors in patients with unruptured intracranial aneurysms: a black-blood MRI study, Interventional neuroradiology : journal of peritherapeutic neuroradiology, surgical procedures and related neurosciences 22 (2016) 501–505, https://doi.org/10.1177/1591019916653252.

[7] P. Labeyrie, R. Goulay, S. Martinez de Lizarrondo, M. Hébert, M. Gauberti, E. Maubert, B. Delaunay, B. Gory, F. Signorelli, F. Turjman, et al., Vascular tissue-type plasminogen activator promotes intracranial aneurysm formation, Stroke 48 (2017) 2574–2582, https://doi.org/10.1161/strokeaha.117.017305.

[8] M. Fu, F. Peng, M. Zhang, S. Chen, H. Niu, X. He, B. Xu, A. Liu, R. Li, Aneurysmal wall enhancement and hemodynamics: pixel-level correlation between spatial distribution, Quant. Imag. Med. Surg. 12 (2022) 3692–3704, https://doi.org/10.21037/qims-21-1203.

[9] M. Zhang, F. Peng, X. Tong, X. Feng, Y. Li, H. Chen, H. Niu, B. Zhang, G. Song, Y. Li, et al., Associations between haemodynamics and wall enhancement of intracranial aneurysm, Stroke and vascular neurology 6 (2021) 467–475, https://doi.org/10.1136/svn-2020-000636.

[10] C. Santarosa, B. Cord, A. Koo, P. Bhogal, A. Malhotra, S. Payabvash, F. Minja, C. Matouk, Vessel wall magnetic resonance imaging in intracranial aneurysms: principles and emerging clinical applications, Interventional neuroradiology : journal of peritherapeutic neuroradiology, surgical procedures and related neurosciences 26 (2020) 135–146, https://doi.org/10.1177/1591019919891297.

[11] M. Vergouwen, D. Backes, I. van der Schaaf, J. Hendrikse, R. Kleinloog, A. Algra, G. Rinkel, Gadolinium enhancement of the aneurysm wall in unruptured intracranial aneurysms is associated with an increased risk of aneurysm instability: a follow-up study, AJNR. American journal of neuroradiology 40 (2019) 1112–1116, https://doi.org/10.3174/ajnr.A6105.

[12] F. Gariel, W. Ben Hassen, G. Boulouis, R. Bourcier, D. Trystram, L. Legrand, C. Rodriguez-Regent, D. Saloner, C. Oppenheim, O. Naggara, M. Edjlali, Increased wall enhancement during follow-up as a predictor of subsequent aneurysmal growth, Stroke 51 (2020) 1868–1872, https://doi.org/10.1161/strokeaha.119.028431.

[13] W. Xiao, T. Qi, S. He, Z. Li, S. Ou, G. Zhang, X. Liu, Z. Huang, F. Liang, Low wall shear stress is associated with local aneurysm wall enhancement on high-resolution MR vessel wall imaging, AJNR. American journal of neuroradiology 39 (2018) 2082–2087, https://doi.org/10.3174/ajnr.A5806.

[14] R. Molenberg, M. Aalbers, A. Appelman, M. Uyttenboogaart, J. van Dijk, Intracranial aneurysm wall enhancement as an indicator of instability: a systematic review and meta-analysis, Eur. J. Neurol. 28 (2021) 3837–3848, https://doi.org/10.1111/ene.15046.

[15] J. Frösen, J. Cebral, A. Robertson, T. Aoki, Flow-induced, inflammation-mediated arterial wall remodeling in the formation and progression of intracranial aneurysms, Neurosurg. Focus 47 (2019) E21, https://doi.org/10.3171/2019.5.Focus19234.

[16] A. Can, R. Du, Association of hemodynamic factors with intracranial aneurysm formation and rupture: systematic review and meta-analysis, Neurosurgery 78 (2016) 510–520, https://doi.org/10.1227/neu.0000000000001083.

[17] M. Khan, V. Toro Arana, C. Rubbert, J. Cornelius, I. Fischer, R. Bostelmann, H. Mijderwijk, B. Turowski, H. Steiger, R. May, A. Petridis, Association between aneurysm hemodynamics and wall enhancement on 3D vessel wall MRI, J. Neurosurg. (2020) 1–11, https://doi.org/10.3171/2019.10.Jns191251.

[18] N. Lv, C. Karmonik, S. Chen, X. Wang, Y. Fang, Q. Huang, J. Liu, Wall enhancement, hemodynamics, and morphology in unruptured intracranial aneurysms with high rupture risk, Translational stroke research 11 (2020) 882–889, https://doi.org/10.1007/s12975-020-00782-4.

[19] H. Meng, V. Tutino, J. Xiang, A. Siddiqui, High WSS or low WSS? Complex interactions of hemodynamics with intracranial aneurysm initiation, growth, and rupture: toward a unifying hypothesis, AJNR. American journal of neuroradiology 35 (2014) 1254–1262, https://doi.org/10.3174/ajnr.A3558.

[20] C. Zhu, H. Haraldsson, B. Tian, K. Meisel, N. Ko, M. Lawton, J. Grinstead, S. Ahn, G. Laub, C. Hess, D. Saloner, High resolution imaging of the intracranial vessel wall at 3 and 7 T using 3D fast spin echo MRI, Magma 29 (2016) 559–570, https://doi.org/10.1007/s10334-016-0531-x.

[21] X. Liu, Z. Zhang, C. Zhu, J. Feng, P. Liu, Q. Kong, X. Zhang, Q. Zhang, H. Jin, H. Ge, et al., Wall enhancement of intracranial saccular and fusiform aneurysms may differ in intensity and extension: a pilot study using 7-T high-resolution black-blood MRI, Eur. Radiol. 30 (2020) 301–307, https://doi.org/10.1007/s00330-019-06275-9.

[22] J. Roa, M. Zanaty, C. Osorno-Cruz, D. Ishii, G. Bathla, S. Ortega-Gutierrez, D. Hasan, E. Samaniego, Objective quantification of contrast enhancement of unruptured intracranial aneurysms: a high-resolution vessel wall imaging validation study, J. Neurosurg. 134 (2020) 862–869, https://doi.org/10.3171/2019.12.Jns192746.

[23] S. Fukuda, Y. Shimogonya, N. Yonemoto, Differences in cerebral aneurysm rupture rate according to arterial anatomies depend on the hemodynamic environment, AJNR. American journal of neuroradiology 40 (2019) 834–839, https://doi.org/10.3174/ajnr.A6030.

[24] R. Dashti, J. Hernesniemi, H. Lehto, M. Niemelä, M. Lehecka, J. Rinne, M. Porras, A. Ronkainen, S. Phornsuwannapha, T. Koivisto, J. Jääskeläinen, Microneurosurgical management of proximal anterior cerebral artery aneurysms, Surg. Neurol. 68 (2007) 366–377, https://doi.org/10.1016/j.surneu.2007.07.084.

[25] J. Cebral, M. Raschi, Suggested connections between risk factors of intracranial aneurysms: a review, Ann. Biomed. Eng. 41 (2013) 1366–1383, https://doi.org/10.1007/s10439-012-0723-0.

[26] M. Markl, A. Frydrychowicz, S. Kozerke, M. Hope, O. Wieben, 4D flow MRI, J. Magn. Reson. Imag. : JMRI 36 (2012) 1015–1036, https://doi.org/10.1002/jmri.23632.

[27] F. Mut, R. Löhner, A. Chien, S. Tateshima, F. Viñuela, C. Putman, J. Cebral, Computational hemodynamics framework for the analysis of cerebral aneurysms, International journal for numerical methods in biomedical engineering 27 (2011) 822–839, https://doi.org/10.1002/cnm.1424.

[28] S. Hadad, F. Mut, B. Chung, J. Roa, A. Robertson, D. Hasan, E. Samaniego, J. Cebral, Regional aneurysm wall enhancement is affected by local hemodynamics: a 7T MRI study, AJNR. American journal of neuroradiology 42 (2021) 464–470, https://doi.org/10.3174/ajnr.A6927.

[29] H. Wang, T. Krüger, F. Varnik, Effects of size and elasticity on the relation between flow velocity and wall shear stress in side-wall aneurysms: a lattice Boltzmann-based computer simulation study, PLoS One 15 (2020) e0227770, https://doi.org/10.1371/journal.pone.0227770.

[30] B. Cornelissen, E. Leemans, C. Slump, R. van den Berg, H. Marquering, C. Majoie, Hemodynamic changes after intracranial aneurysm growth, J. Neurosurg. (2021) 1–7, https://doi.org/10.3171/2021.6.Jns204155.

[31] E. Nordahl, S. Uthamaraj, K. Dennis, A. Sejkorová, A. Hejčl, J. Hron, H. Švihlová, K. Carlson, Y. Suzen, D. Dragomir-Daescu, Morphological and hemodynamic changes during cerebral aneurysm growth, Brain Sci. 11 (2021), https://doi.org/10.3390/brainsci11040520.

[32] S. Soldozy, P. Norat, M. Elsarrag, A. Chatrath, J. Costello, J. Sokolowski, P. Tvrdik, M. Kalani, M. Park, The biophysical role of hemodynamics in the pathogenesis of cerebral aneurysm formation and rupture, Neurosurg. Focus 47 (2019) E11, https://doi.org/10.3171/2019.4.Focus19232.

[33] D. Sforza, C. Putman, J. Cebral, Hemodynamics of cerebral aneurysms, Annu. Rev. Fluid Mech. 41 (2009) 91–107, https://doi.org/10.1146/annurev.fluid.40.111406.102126.

[34] H. Meng, Z. Wang, Y. Hoi, L. Gao, E. Metaxa, D. Swartz, J. Kolega, Complex hemodynamics at the apex of an arterial bifurcation induces vascular remodeling resembling cerebral aneurysm initiation, Stroke 38 (2007) 1924–1931, https://doi.org/10.1161/strokeaha.106.481234.

[35] E. Metaxa, M. Tremmel, S. Natarajan, J. Xiang, R. Paluch, M. Mandelbaum, A. Siddiqui, J. Kolega, J. Mocco, H. Meng, Characterization of critical hemodynamics contributing to aneurysmal remodeling at the basilar terminus in a rabbit model, Stroke 41 (2010) 1774–1782, https://doi.org/10.1161/strokeaha.110.585992.

[36] P. Lasjaunias, R. Piske, K. Terbrugge, R. Willinsky, Cerebral arteriovenous malformations (C. AVM) and associated arterial aneurysms (AA). Analysis of 101 C. AVM cases, with 37 AA in 23 patients, Acta Neurochir. 91 (1988) 29–36, https://doi.org/10.1007/bf01400524.

[37] P. Jiang, Q. Liu, J. Wu, X. Chen, M. Li, F. Yang, Z. Li, S. Yang, R. Guo, B. Gao, et al., Hemodynamic findings associated with intraoperative appearances of intracranial aneurysms, Neurosurg. Rev. 43 (2020) 203–209, https://doi.org/10.1007/s10143-018-1027-0.

[38] S. Sugiyama, H. Endo, K. Niizuma, T. Endo, K. Funamoto, M. Ohta, T. Tominaga, Computational hemodynamic analysis for the diagnosis of atherosclerotic changes in intracranial aneurysms: a proof-of-concept study using 3 cases harboring atherosclerotic and nonatherosclerotic aneurysms simultaneously, Comput. Math. Methods Med. 2016 (2016) 2386031, https://doi.org/10.1155/2016/2386031.
[39] R. Blankena, R. Kleinloog, B. Verweij, P. van Ooij, B. Ten Haken, P. Luijten, G. Rinkel, J. Zwanenburg, Thinner regions of intracranial aneurysm wall correlate with regions of higher wall shear stress: a 7T MRI study, AJNR. American journal of neuroradiology 37 (2016) 1310–1317, https://doi.org/10.3174/ajnr.A4734.
[40] K. Mizoi, T. Yoshimoto, Y. Nagamine, Types of unruptured cerebral aneurysms reviewed from operation video-recordings, Acta Neurochir. 138 (1996) 965–969, https://doi.org/10.1007/bf01411286.
[41] Q. Liu, Y. Zhang, J. Yang, Y. Yang, M. Li, S. Chen, P. Jiang, N. Wang, Y. Zhang, J. Liu, et al., The relationship of morphological-hemodynamic characteristics, inflammation, and remodeling of aneurysm wall in unruptured intracranial aneurysms, Translational stroke research 13 (2022) 88–99, https://doi.org/10.1007/s12975-021-00917-1.
[42] M. Xu, N. Lv, K. Sun, R. Hong, H. Wang, X. Wang, L. Xu, L. Chen, M. Xu, Morphological and hemodynamic risk factors for the rupture of proximal anterior cerebral artery aneurysms (A1 segment), Front. Aging Neurosci. 14 (2022) 835373, https://doi.org/10.3389/fnagi.2022.835373.
[43] A. Morita, T. Kirino, K. Hashi, N. Aoki, S. Fukuhara, N. Hashimoto, T. Nakayama, M. Sakai, A. Teramoto, S. Tominari, T. Yoshimoto, The natural course of unruptured cerebral aneurysms in a Japanese cohort, N. Engl. J. Med. 366 (2012) 2474–2482, https://doi.org/10.1056/NEJMoa1113260.
[44] Y. Zhang, G. Zhou, W. Liu, W. Gu, Y. Zhu, L. Meng, L. Wei, M. Li, H. Lu, G. Teng, Analysis of risk factors for anterior communicating artery aneurysm rupture: a single-center study, World neurosurgery 153 (2021) e59–e65, https://doi.org/10.1016/j.wneu.2021.06.007.
[45] M. Castro, C. Putman, M. Sheridan, J. Cebral, Hemodynamic patterns of anterior communicating artery aneurysms: a possible association with rupture, AJNR. American journal of neuroradiology 30 (2009) 297–302, https://doi.org/10.3174/ajnr.A1323.
[46] S. Asari, T. Ohmoto, Long-term outcome of surgically treated unruptured cerebral aneurysms, Clin. Neurol. Neurosurg. 96 (1994) 230–235, https://doi.org/10.1016/0303-8467(94)90074-4.